Int. J. Solids Structures Vol. 29, No. 18, pp. 2235–2258, 1992
Printed in Great Britain.

0020-7683/92 $5.00 + .00

ANALYTICAL MODELLING OF SECOND ORDER EFFECTS IN LARGE DEFORMATION PLASTICITY

R. KHEN† and M. B. RUBIN
Faculty of Mechanical Engineering, Technion—Israel Institute of Technology,
32000 Haifa, Israel

(*Received* 18 *July* 1991; *in revised form* 8 *January* 1992)

Abstract—Nonlinear constitutive equations for an elastically isotropic elastic–viscoplastic material have been used to predict the second order effects that cause axial elongation during pure shear, normal stresses during simple shear and accumulated axial elongation during cyclic pure shear. Specific attention has been focused on the determination of material constants for OFE copper and 70:30 α brass by matching the stress–strain curve for large deformation torsion and the second order effect of axial elongation observed during torsion without axial constraint. The results of this paper indicate that second order effects in the plastic region are driven by second order elastic effects that cause small terms to appear in the flow rule which continue to influence the accumulation of plastic deformation. These second order elastic effects are mainly controlled by a single material constant C_2 that can be determined by experimentation.

1. INTRODUCTION

Poynting (1909) studied second order effects in the elastic range by considering torsion of solid wires with and without axial constraint. From his experiments Poynting concluded that axial elongation occurs under torsion without axial constraint and axial compressive stresses are created under torsion with axial constraint. Later, Swift (1947) showed that this elongation persists in the plastic range and that upon load reversal the elongation decreases slightly even while reverse plastic loading occurs and then continues to increase causing a net increase in length. Freudenthal and Ronay (1966) exploited the fact that elongation persists in the plastic range and studied the accumulated increase in length caused by a large number of torsional cycles of small amplitude. All of these effects are termed second order effects because they are absent in solutions based on the small deformation theory.

Recently, Harren *et al.* (1989) have reviewed a number of both phenomenological and crystal plasticity analyses of the Swift effect. In their review Harren *et al.* (1989) also analysed the Swift effect mainly using a rate-dependent model for polycrystals that includes detailed effects of texture evolution. Although their prediction of the magnitude of the Swift effect is significantly exaggerated they are able to qualitatively predict the decrease in elongation during reverse plastic loading observed by Swift (1947), which is an effect attributed to texture evolution.

The objective of this paper is to develop specific simple constitutive equations for large deformation of elastic–viscoplastic metals which can be used to model these second order effects. These specific constitutive equations represent a synthesis of developments over the last few years. The general theory for elastic–viscoplastic materials (Rubin, 1986) has been developed using the kinematics suggested by Green and Naghdi (1965, 1966) for large deformation of elastic–plastic materials and is consistent with the thermodynamic procedures proposed more recently by them (Green and Naghdi, 1977, 1978). The specific equations model an elastically isotropic elastic–viscoplastic metal and do not model texture effects. Viscoplasticity is introduced in these equations by modifying the flow rule for plastic deformation and the hardening equations starting with the work by Bodner and Partom (1972, 1975) and Bodner (1985). The resulting equations for viscoplasticity are specific examples of equations associated with a unified theory without a yield surface [e.g. Bodner

† Formerly named R. Chen.

(1987)]. The functional forms of the equations have been developed to model high compression caused by shock waves (Rubin, 1987a, 1990) and the equations also model very large shearing because the theory exhibits a continuity of solid and fluid states (Rubin, 1987b). Another important feature of these equations is that they use kinematics which separate the effect of elastic dilatation (volume change) from that of elastic distortion. This separation, which is used here for an elastic–plastic response was introduced by Flory (1961) for elastic response. More specifically, the distortional strain energy depends on the dilatation and on two scalar measures of pure elastic distortion proposed by Rubin (1987b) and denoted by β_1, β_2. These scalars β_1, β_2 are the two independent invariants of the inverse $\mathbf{C}_e'^{-1}$ of the unimodular tensor $\mathbf{C}_e'$ characterizing the elastic distortion discussed by Rubin and Chen (1991).

The elastic response exhibited by these specific constitutive equations is characterized by five independent material constants:

$$\{K_0, \mu_0\}, \qquad \{s_1, m_p, C_2\}. \tag{1a, b}$$

The first two constants (1a) are associated with first order effects and can be determined by the small deformation theory. Specifically, K_0 is the reference value of the bulk modulus and μ_0 is the reference value of the shear modulus. The remaining three constants (1b) are associated with second order effects which cannot be determined by the small deformation theory. Specifically, s_1 characterizes the nonlinear dependence of pressure on dilatation (volume change); m_p characterizes the dependence of the shear modulus on dilatation parametrically through a part of the pressure; and C_2 controls higher order effects of elastic distortion in the distortional strain energy.

It will be shown that the values of the second order constants (1b) do not significantly influence the first order response. Consequently, the procedures for determining the first and second order constants are uncoupled. In particular, values for the first order constants (1a) can be determined by acoustic bulk and shear wave speeds, and values for the second order constants can be determined by matching second order effects directly. Alternatively, it has been shown (Rubin, 1990) that the five elastic constants (1) are determined in terms of the more common constants associated with a Taylor series expansion of the strain energy including third order terms. Furthermore, this uncoupling of first and second order constants should be contrasted with other work [e.g. Im and Atluri (1987), Figs 6, 7] where the material constant that controls the second order response of axial elongation also influences the first order response of shear stress versus shear strain.

Here, the values for s_1, m_p are determined by shock wave data. Although the constant C_2 can in principle be determined by an elastic experiment, nonlinearities in the elastic response are usually difficult to measure for metals in which the elastic strain remains very small. However, since here we show that the value of C_2 significantly influences the accumulated value of axial elongation during torsion into the plastic region it is more convenient to determine the value of C_2 by matching the value of elongation measured by Swift (1947).

For definiteness, let $\{T_{rr}, T_{\theta\theta}, T_{zz}, T_{r\theta}, T_{rz}, T_{\theta z}\}$ be the independent (apart from symmetry) physical components of the Cauchy stress $\mathbf{T}$ referred to the orthonormal base vectors $\{\mathbf{e}_r, \mathbf{e}_\theta, \mathbf{e}_z\}$ associated with a cylindrical polar coordinate system. In the study of constitutive properties of materials it has become common to perform torsion experiments on thin hollow tubes. If the tubes are extremely thin then the deformation can be approximated as homogeneous and the experimental results can be easily interpreted. Unfortunately, in order to avoid buckling in a finite deformation torsion experiment on a hollow tube, it is necessary to make the thickness of the tube be at least 10–15% of the mean radius. Therefore, these hollow tubes cannot really be considered to be thin and the deformation is not really homogeneous. In spite of this fact, if one is only interested in first order effects, then torsional experiments on these hollow tubes with no axial constraint can be considered to create relatively homogeneous deformation and a state of pure shear in which the only nonzero independent component of the Cauchy stress is $T_{\theta z}$. However, it is important to emphasize that if one is interested in second order effects such as the elongation

caused by pure torsion, then the inhomogeneity of the deformation in even thin hollow tubes is itself a second order effect that can significantly influence other second order effects of interest.

More specifically, we note that since the amount of shear in a torsion experiment increases with increasing radius, the axial elongation also tends to increase with increasing radius. This effect tends to cause the shear stress T_{rz} to develop. Also, by thinking of the thin tube as a collection of thinner concentric tubes we can expect that the second order effect of this variation of shear would tend to cause changes in the radii of the concentric tubes. However, since these concentric tubes are kinematically coupled, the variation of shear tends to cause nonzero stress components T_{rr} and $T_{\theta\theta}$ to develop. As mentioned above, these complicating features are all second order effects that can significantly influence the measurement of other second order effects. In particular, Swift (1947) observed that hollow tubes (of 70:30 α brass) under torsion with no axial constraint tend to extend about 50% further than solid bars under the same loading. Ronay (1968) observed that this difference is even more pronounced on the accumulated elongation due to small amplitude cyclic torsional loading. For the smaller torsion angles ($<3^\circ$) the elongations of hollow tubes were as much as eight times those of the solid bars, whereas for the larger torsion angles ($\approx 30^\circ$) the elongations of hollow tubes were nearly the same as for solid bars. Freudenthal and Ronay (1966) also observed that even a small axial tension can significantly increase the accumulated elongation due to cyclic torsional loading. It is therefore reasonable to assume that the radial constraint associated with grasping the ends of a hollow tube may also influence the measurement of second order effects. Thus, torsion of solid bars or even hollow tubes that are thick enough not to buckle cannot provide clean experimental data for determining second order effects in the constitutive response.

Since accurate machining of thin hollow tubes is relatively difficult, most of the experiments performed by Swift (1947) and Freudenthal and Ronay (1966) were performed on solid bars. In view of the complications discussed above, a complete analysis of second order effects in a solid bar would require implementing the proposed model in an appropriate large deformation computer code and numerically solving the inhomogeneous problem. This approach was taken by Lipkin *et al.* (1988) using a different set of constitutive equations than those proposed here.

Instead of programing these constitutive equations in a large deformation computer program to obtain accurate quantitative comparison with experimental data, the usual procedure of considering the simpler homogeneous problem of pure shear in a rectangular Cartesian coordinate system is followed, even though at this time we cannot quantitatively assess the error in this procedure. More specifically, let T_{ij} $(i = 1, 2, 3)$ be the components of the Cauchy stress referred to a rectangular Cartesian coordinate system with the orthonormal base vectors $\{\mathbf{e}_1, \mathbf{e}_2, \mathbf{e}_3\}$. In this paper pure shear in the $\mathbf{e}_1$–$\mathbf{e}_2$ plane is considered, with the only nonzero independent component of stress being T_{12}. First order correspondence with the physical experiment can be obtained by identifying the Cartesian directions $\{\mathbf{e}_1, \mathbf{e}_2, \mathbf{e}_3\}$ with the cylindrical polar directions $\{\mathbf{e}_\theta, \mathbf{e}_z, \mathbf{e}_r\}$.

The following analysis shows that the value of C_2 significantly influences the elongation in the $\mathbf{e}_2$ direction caused by shear in the $\mathbf{e}_1$–$\mathbf{e}_2$ plane and can therefore be determined by measurements of elongation in a clean experiment. In this paper a value of C_2 is determined for 70:30 α brass by quantitatively matching theoretical predictions with the elongation measured by Swift (1947) in an experiment on a hollow tube. Also, a value of C_2 is determined for copper by matching a pseudo experimental curve of elongation in a hollow tube which was obtained using the approximation discussed by Swift (1947) which increases the elongation measured for a solid bar by 50%.

Although texture development due to large plastic deformation significantly influences the magnitude of axial elongation for very large shear strains, it is shown here that for moderate strains this axial elongation can be modelled by a theory that does not include texture development. The nonrecoverable nature of axial elongation during torsion into the plastic region is of course due to the plastic response. However, it should be emphasized that the results of this paper indicate that second order effects in the plastic region are driven by second order elastic effects that cause small terms to appear in the flow rule which

continue to influence the accumulation of plastic deformation. These second order effects are mainly controlled by the elastic constant C_2. In this regard it is important that the constitutive equations used to model axial elongation be of the hyperelastic type (for which a strain energy function exists) so that they properly model nonlinear elastic response. Furthermore, we mention that for convenience, the present analysis uses a viscoplastic theory without a yield surface. However, the major results obtained here could also be obtained using a rate-independent theory of plasticity with a yield surface developed by modifying the flow rule (Rubin, 1989).

In the following sections we review the basic constitutive equations and discuss results for small elastic distortions and the formulation for pure shear. Next, it is shown how to determine the first order material constants characterizing elastic and plastic response. Then the procedure for determining the second order elastic constants is presented. Additional simulations of simple shear and the accumulated axial elongation due to cyclic torsional loading without axial constraint are presented, and a conclusion section is included to summarize the main results. Furthermore, for the convenience of the reader a number of detailed mathematical developments are included in four appendices.

2. BASIC CONSTITUTIVE EQUATIONS

In this section we briefly recall constitutive equations for the purely mechanical response of an elastically isotropic elastic–viscoplastic material. These constitutive equations were used by Chen (1990) to study second order effects and they may be obtained by specializing the equations used by Rubin (1990) for viscoplasticity in 6061-T6 aluminum.

For background information, let $\mathbf{X}$ denote the position of a material point in the reference configuration and $\mathbf{x}$ denote the position of the same material point in the present configuration at time t. Also, let $\mathbf{F} = \partial\mathbf{x}/\partial\mathbf{X}$ be the deformation gradient, $\mathbf{C} = \mathbf{F}^{\mathrm{T}}\mathbf{F}$ be the total deformation, $\mathbf{C}_{\mathrm{p}}$ be a symmetric positive definite tensor denoting the plastic deformation and $\mathbf{S}$ be the symmetric Piola–Kirchhoff stress. For the purely mechanical theory the temperature θ is assumed to remain equal to its reference value θ_0 and the expression for the specific (per unit mass) Helmholtz free energy ψ given in Rubin (1990) reduces to

$$\psi = \psi_1(I_3) + \psi'(I_3, \beta_1, \beta_2), \qquad 2\rho_0\psi_1 = f_2(I_3), \tag{2a, b}$$

$$2\rho_0\psi' = \hat{\mu}(I_3)[C_1(\beta_1 - 3) + C_2(\beta_2 - 3)], \qquad C_1 + 4C_2 = 1, \tag{2c, d}$$

$$2\rho_0\psi' = \hat{\mu}(I_3)[(1 - 4C_2)(\beta_1 - 3) + C_2(\beta_2 - 3)], \tag{2e}$$

where ρ_0 is the mass density in the reference configuration, I_3 is a pure measure of dilatation and β_1, β_2 are pure measures of elastic distortional deformation defined in Rubin (1987b) by

$$\beta_1 = \left(\frac{I_3}{I_{3\mathrm{p}}}\right)^{1/3}(\mathbf{C}^{-1}\cdot\mathbf{C}_{\mathrm{p}}), \qquad \beta_2 = \left(\frac{I_3}{I_{3\mathrm{p}}}\right)^{2/3}(\mathbf{C}_{\mathrm{p}}\mathbf{C}^{-1}\cdot\mathbf{C}^{-1}\mathbf{C}_{\mathrm{p}}), \tag{3a, b}$$

$$I_3 = \det\mathbf{C}, \qquad I_{3\mathrm{p}} = \det\mathbf{C}_{\mathrm{p}} = 1. \tag{3c, d}$$

In (3) and throughout the text the notation $\mathbf{A}\cdot\mathbf{B} = \mathrm{tr}(\mathbf{A}\mathbf{B}^{\mathrm{T}})$ denotes the inner product between two second order tensors. The term ψ_1 represents the free energy due to purely hydrostatic loading and the term ψ' represents the free energy due to elastic distortion. The function $\hat{\mu}$ is related to the effective shear modulus μ by the formula (Rubin, 1987a):

$$\hat{\mu}(I_3) = I_3^{1/2}\mu(I_3), \tag{4}$$

and (3d) represents the condition of plastic incompressibility. The constants C_1 and C_2 in (2c) control the influences of the measures of elastic distortion β_1 and β_2, respectively. Furthermore, β_1 and β_2 are exact measures which have not been approximated using a

Taylor series expansion so the terms (β_1-3) and (β_2-3) are not purely quadratic in strain and each one of them influences both first and second order elastic response. Consequently, to ensure that for small elastic distortions the shear modulus attains the value μ_0, the constants C_1 and C_2 must be dependent and satisfy the restriction (2d) [see Rubin (1987b)]. For convenience we solve (2d) for C_1 and substitute the result into (2c) to obtain (2e). It follows that C_2 in (2e) is a second order material constant because it does not influence first order effects. Later, it will be shown that C_2 in (2e) controls the Swift effect (Chen, 1990).

For the class of constitutive equations considered here it can be shown (Rubin, 1987a) using the procedures proposed by Green and Naghdi (1977, 1978) that the stress S and a part ξ' of the internal rate of production of entropy related to plastic dissipation may be expressed in terms of derivatives of the Helmholtz free energy. Specifically, for the purely mechanical theory equations (4a–e, 1) in Rubin (1990) reduce to

$$\mathbf{S} = 2\rho_0\left(\frac{\partial\psi}{\partial\mathbf{C}}\right) = -pI_3^{1/2}\mathbf{C}^{-1}+\mathbf{S}', \qquad p = p_1(I_3)+p'(I_3,\beta_1,\beta_2), \tag{5a, b}$$

$$p_1 = -I_3^{1/2}\left(\frac{\mathrm{d}f_2}{\mathrm{d}I_3}\right), \qquad p' = -I_3^{1/2}\left(\frac{\mathrm{d}\hat{\mu}}{\mathrm{d}I_3}\right)[(1-4C_2)(\beta_1-3)+C_2(\beta_2-3)], \tag{5c, d}$$

$$\mathbf{S}' = -(1-4C_2)I_3^{1/3}\hat{\mu}[\mathbf{C}^{-1}\mathbf{C}_p\mathbf{C}^{-1}-\tfrac{1}{3}(\mathbf{C}^{-1}\cdot\mathbf{C}_p)\mathbf{C}^{-1}]-2C_2I_3^{2/3}\hat{\mu}[\mathbf{C}^{-1}\mathbf{C}_p\mathbf{C}^{-1}\mathbf{C}_p\mathbf{C}^{-1} - \tfrac{1}{3}(\mathbf{C}_p\mathbf{C}^{-1}\cdot\mathbf{C}^{-1}\mathbf{C}_p)\mathbf{C}^{-1}], \tag{5e}$$

$$\rho_0\theta\xi' = -\rho_0\left(\frac{\partial\psi}{\partial\mathbf{C}_p}\right)\cdot\dot{\mathbf{C}}_p = -\frac{\hat{\mu}}{2}[(1-4C_2)I_3^{1/3}\mathbf{C}^{-1}+2C_2I_3^{2/3}\mathbf{C}^{-1}\mathbf{C}_p\mathbf{C}^{-1}]\cdot\dot{\mathbf{C}}_p. \tag{5f}$$

In (5), the total pressure p is composed of a part p_1 dependent on dilatation only and a part p' dependent on dilatation and elastic distortion. Also, a superposed dot denotes material time differentiation holding $\mathbf{X}$ fixed and the Cauchy stress $\mathbf{T}$ and its deviatoric part $\mathbf{T}'$ are given by

$$\mathbf{T} = -p\mathbf{I}+\mathbf{T}', \qquad \mathbf{T}' = I_3^{-1/2}\mathbf{F}\mathbf{S}'\mathbf{F}^{\mathrm{T}}, \tag{6a, b}$$

where $\mathbf{I}$ is the unity tensor.

For high compression applications including thermal effects Rubin (1987a) determined the function f_2 by matching a Mie–Gruneisen equation for the pressure p_1. Since here we are confining our attention to the purely mechanical response it is sufficient to assume that the pressure p_1 is equal to the Hugoniot pressure p_H such that

$$p_1 = p_H(I_3) = \frac{K_0\phi}{(1-s_1\phi)^2}, \qquad K_0 = \rho_0 C_0^2, \tag{7a, b}$$

where C_0 is the bulk wave speed, s_1 is a constant, and the total compression ϕ is defined by

$$\phi = 1-I_3^{1/2}. \tag{8}$$

Substituting (7a) into (5c) and requiring the dilatational energy ψ_1 to vanish in the reference configuration [i.e. $\psi_1(1) = 0$] it follows that

$$f_2(I_3) = \frac{2K_0}{s_1^2}\left[\frac{1}{(1-s_1\phi)}+\ln(1-s_1\phi)-1\right]. \tag{9}$$

In addition, the effective shear modulus μ in (4) is determined by the expression

$$\mu(I_3) = \mu_0[(1-C_\mu)I_3^{-1/2} + C_\mu(1+m_p I_3^{1/6} p_1)]. \tag{10}$$

For convenience we have introduced C_μ to distinguish between the two cases when C_μ takes the values zero and unity. When C_μ vanishes, $\hat{\mu}$ in (4) equals the constant value μ_0; the part ψ' of the Helmholtz free energy depends only on elastic distortion; and the pressure p depends only on the dilatation I_3 [$p' = 0$]. Alternatively, when C_μ equals unity, the dependence of μ on pressure is controlled by the constant m_p, $\hat{\mu}$ in (4) depends on dilatation, the distortional part ψ' of the Helmholtz free energy also depends on dilatation, and the pressure includes a term p' which depends on elastic distortion. Furthermore, when C_μ equals unity the expression (10) reduces to a form similar to the one proposed by Steinberg *et al.* (1980) when the temperature dependence of μ is neglected.

The equations (2)–(10) determine the elastic response. The plastic response is characterized by the flow rule (Rubin, 1987b)

$$\dot{\mathbf{C}}_p = \Gamma \mathbf{A}, \qquad \mathbf{A} = \left(\frac{3}{\mathbf{C}_p^{-1}\cdot\mathbf{C}}\right)\mathbf{C} - \mathbf{C}_p, \tag{11a, b}$$

which is a constitutive equation for the rate of plastic deformation $\dot{\mathbf{C}}_p$, and by evolution equations for the rate of hardening. The specific form of Γ used here,

$$\Gamma = \Gamma_0 \exp\left[-\tfrac{1}{2}\left(\frac{Z}{\sigma_e}\right)^{2n}\right], \tag{12}$$

was introduced by Rubin (1987b, with $R = 1$) as a modified form of the viscoplastic flow rule proposed by Bodner and Partom (1972, 1975). In (12) Γ_0 and n are constants, σ_e is the von Mises stress defined by

$$\sigma_e^2 = \tfrac{3}{2}\mathbf{T}'\cdot\mathbf{T}', \tag{13}$$

and Z is a measure of hardening that is separated additively into a measure κ of isotropic hardening and a scalar measure β of directional hardening such that

$$Z = \kappa + \beta. \tag{14}$$

The scalar β is related to the tensorial measure $\boldsymbol{\beta}$ of directional hardening by the formulae

$$\beta = \mathbf{C}_p^{-1}\boldsymbol{\beta}\cdot\mathbf{U}\mathbf{C}_p^{-1}, \qquad \mathbf{U} = \frac{\mathbf{A}}{(\mathbf{C}_p^{-1}\mathbf{A}\cdot\mathbf{A}\mathbf{C}_p^{-1})^{1/2}}, \tag{15a, b}$$

and the evolution equations for κ and $\boldsymbol{\beta}$ are specified by

$$\dot{\kappa} = m_1(\rho_0\theta\xi')(Z_1 - \kappa), \qquad \dot{\boldsymbol{\beta}} = m_2(\rho_0\theta\xi')(Z_3\mathbf{U} - \boldsymbol{\beta}). \tag{16a, b}$$

In (16) the constant Z_1 denotes the saturated value of κ, and the constant Z_3 denotes the saturated value of β. For background information, we note that the directional hardening tensor $\boldsymbol{\beta}$ was introduced by Bodner (1985) to model the Bauschinger effect and is an alternative to kinematic hardening. However, the definitions (15a, b) are modified versions of the ones used by Bodner (1985).

The differential equations (11a), (16a,b) determine the values of $\mathbf{C}_p$, κ, $\boldsymbol{\beta}$ and may be integrated subject to initial conditions. Here we assume that in the reference configuration $\mathbf{C}_p$, κ, $\boldsymbol{\beta}$ are given by

$$\mathbf{C}_p = \mathbf{I}, \qquad \kappa = \kappa_0, \qquad \beta = 0, \tag{17a, b, c}$$

where κ_0 is a constant.

The quantities m_1 and m_2 in (16a, b) control the rate of hardening and are usually taken to be constants (Bodner, 1985). However, in order to more closely model the nonlinear hardening exhibited by some metals like copper we assume here that m_2 is constant but that m_1 is a function of κ of the form

$$m_1(\kappa) = mb + (ma - mb)\exp[-mc(\kappa - \kappa_0)], \tag{18}$$

where ma, mb, mc are non-negative constants. It follows from (18) that m_1 decreases from the value ma towards the value mb as the material hardens and κ increases. This has the desired effect of slowing down the rate at which κ approaches its saturated value.

3. SMALL ELASTIC DISTORTION

In this section we develop certain useful formulae that are valid for small elastic distortion. To this end, it is desirable to define a measure $\mathbf{B}_e$ of elastic deformation, a measure $\mathbf{B}_e'$ of elastic distortional deformation, and a measure $\mathbf{g}_e'$ of elastic distortional strain such that

$$\mathbf{B}_e = \mathbf{F}\mathbf{C}_p^{-1}\mathbf{F}^T, \qquad \mathbf{B}_e' = \left(\frac{I_3}{I_{3p}}\right)^{-1/3}\mathbf{B}_e, \qquad \det \mathbf{B}_e' = 1, \qquad \mathbf{g}_e' = \tfrac{1}{2}(\mathbf{I} - \mathbf{B}_e'^{-1}). \tag{19a, b, c, d}$$

Then with the help of (3d), (4), (5e), (6b) and (19) we may rewrite the deviatoric Cauchy stress $\mathbf{T}'$ in the forms:

$$\mathbf{T}' = -\mu[(1 - 4C_2)\{\mathbf{B}_e'^{-1} - \tfrac{1}{3}(\mathbf{B}_e'^{-1}\cdot\mathbf{I})\mathbf{I}\} + 2C_2\{\mathbf{B}_e'^{-2} - \tfrac{1}{3}(\mathbf{B}_e'^{-2}\cdot\mathbf{I})\mathbf{I}\}], \tag{20a}$$

$$\mathbf{T}' = 2\mu[\{\mathbf{g}_e' - \tfrac{1}{3}(\mathbf{g}_e'\cdot\mathbf{I})\mathbf{I}\} - 4C_2\{\mathbf{g}_e'^2 - \tfrac{1}{3}(\mathbf{g}_e'^2\cdot\mathbf{I})\mathbf{I}\}]. \tag{20b}$$

For small elastic distortion the strain $\mathbf{g}_e'$ is assumed to be a small quantity of order ε [denoted by $O(\varepsilon)$, with $0 < \varepsilon \ll 1$] so that

$$\mathbf{B}_e' = \mathbf{I} + O(\varepsilon), \qquad \mathbf{C}_p = \mathbf{C}' + O(\varepsilon), \tag{21a, b}$$

where $\mathbf{C}'$ is the distortional part of $\mathbf{C}$ defined by

$$\mathbf{C}' = I_3^{-1/3}\mathbf{C}, \qquad \det \mathbf{C}' = 1. \tag{22a, b}$$

Therefore, with the help of results in Appendix A, it follows from (20b) and (A3) that for small elastic distortion

$$\mathbf{T}' \approx 2\mu\mathbf{g}_e'. \tag{23}$$

Since the flow rule (11) is consistent with the assumption that plastic deformation is incompressible (3d) it may be shown that

$$\dot{I}_{3p} = I_{3p}\mathbf{C}_p^{-1}\cdot\dot{\mathbf{C}}_p = 0. \tag{24}$$

Thus, using (5e) and (24) the rate of plastic dissipation (5f) may be rewritten in the form:

$$\rho_0\theta\xi' = \mathbf{C}_p^{-1}\mathbf{C}\mathbf{S}' \cdot \tfrac{1}{2}\dot{\mathbf{C}}_p. \tag{25}$$

Alternatively, we may solve (6b) for $\mathbf{S}'$, substitute the result into (25) and use the definition (19b) to obtain the expression

$$\rho_0\theta\xi' = I_3^{\frac{1}{3}}\mathbf{B}_e'\mathbf{T}' \cdot \tfrac{1}{2}(\mathbf{F}'^{-T}\dot{\mathbf{C}}_p\mathbf{F}'^{-1}), \tag{26}$$

where $\mathbf{F}'^{-T}$ denotes the transpose of the inverse of $\mathbf{F}'$ and the distortional part $\mathbf{F}'$ of the deformation gradient is defined (Flory, 1961) by

$$\mathbf{F}' = I_3^{-\frac{1}{6}}\mathbf{F}, \qquad \det \mathbf{F}' = 1. \tag{27a, b}$$

Then, with the help of (13), (21a) and (B7) of Appendix B the rate of plastic dissipation (26) may be approximated by

$$\rho_0\theta\xi' \approx I_3^{\frac{1}{3}}\sigma_e\dot{\varepsilon}_p, \tag{28}$$

where the equivalent plastic strain rate $\dot{\varepsilon}_p$ is defined by (B4).

4. PURE AND SIMPLE SHEAR

Letting X_A and x_i be the Cartesian components of $\mathbf{X}$ and $\mathbf{x}$, respectively, the homogeneous total deformation associated with either pure or simple shear in the $\mathbf{e}_1$–$\mathbf{e}_2$ plane may be expressed in the form

$$x_1 = a(X_1 + \gamma X_2), \qquad x_2 = bX_2, \qquad x_3 = cX_3, \tag{29a, b, c}$$

where a, b, c are quantities to be determined for pure shear and specified for simple shear and γ is a measure of shear (see Fig. 1). Using (3c) and (29) the Cartesian components F_{iA} of $\mathbf{F}$, C_{AB} of $\mathbf{C}$, and the dilatation I_3 become

$$\mathbf{F} = \begin{pmatrix} a & a\gamma & 0 \\ 0 & b & 0 \\ 0 & 0 & c \end{pmatrix}, \qquad \mathbf{C} = \begin{pmatrix} a^2 & a^2\gamma & 0 \\ a^2\gamma & b^2 + a^2\gamma^2 & 0 \\ 0 & 0 & c^2 \end{pmatrix}, \qquad I_3 = (abc)^2. \tag{30a, b, c}$$

With reference to torsion of a thin hollow tube of mean radius r, height h, thickness w in the present configuration, the quantities a, b, c may be approximated by

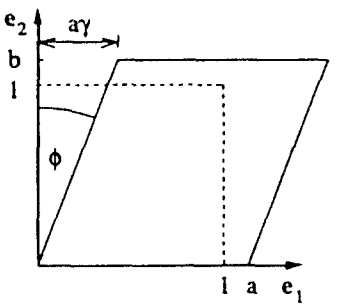

Fig. 1. Pure shear of an element.

$$a = \frac{r}{R}, \qquad b = \frac{h}{H}, \qquad c = \frac{w}{W}, \tag{31a, b, c}$$

where R, H, W are the reference values of r, h, w, respectively. Furthermore, letting θ denote the relative torsion angle between the ends of the tube, and ϕ denote the shear angle (see Fig. 1), the shear measure γ is determined by the equations

$$\tan\phi = \frac{a\gamma}{b} = \frac{r\theta}{h} = \frac{aR\theta}{bH}, \qquad \gamma = \frac{R\theta}{H}. \tag{32a, b}$$

Consequently, each of the quantities a, b, c, γ may be approximated by experimentally observable quantities.

With the help of (17a) and (30) it may be shown that the flow rule (11) permits the plastic deformation to be expressed in the form:

$$\mathbf{C}_p = \begin{bmatrix} a_p^2 & a_p^2\gamma_p & 0 \\ a_p^2\gamma_p & b_p^2 + a_p^2\gamma_p^2 & 0 \\ 0 & 0 & \dfrac{1}{a_p^2 b_p^2} \end{bmatrix}, \tag{33}$$

where a_p, b_p, γ_p are quantities determined in terms of the specified motion $\gamma(t)$ by integrating the three independent scalar equations associated with the flow rule (11) subject to the initial condition (17a). Then (19a), (30a) and (33) may be used to obtain

$$\mathbf{B}_e^{-1} = \begin{bmatrix} \left(\dfrac{a_p}{a}\right)^2 & -\left(\dfrac{a_p^2}{ab}\right)\gamma_e & 0 \\ -\left(\dfrac{a_p^2}{ab}\right)\gamma_e & \dfrac{1}{b^2}[b_p^2 + a_p^2\gamma_e^2] & 0 \\ 0 & 0 & \dfrac{1}{(a_p b_p c)^2} \end{bmatrix}, \qquad \gamma_e = \gamma - \gamma_p, \tag{34a, b}$$

where γ_e is the elastic shear strain. Therefore, with the help of (20) and (34) it follows that for these deformations

$$T'_{13} = 0, \qquad T'_{23} = 0, \tag{35a, b}$$

are satisfied identically.

For pure shear the quantities a, b, c are determined by satisfying the conditions

$$p = 0, \qquad T'_{11} = 0, \qquad T'_{33} = 0, \tag{36a, b, c}$$

where we note that any two of the components T'_{11}, T'_{22}, T'_{33} could have been chosen since $\mathbf{T}'$ is a deviatoric tensor. Furthermore, it was shown in Rubin and Chen (1991) that general constitutive equations for an elastically isotropic elastic–viscoplastic material satisfy the universal relation

$$\mathbf{B}_e\mathbf{T} = \mathbf{T}\mathbf{B}_e \tag{37}$$

for all deformations. It follows by multiplying both sides of (20a) by $\mathbf{B}_e^{-1}$, and using (6a) and (19b) that an equivalent relationship becomes

$$\mathbf{B}_e^{-1}\mathbf{T}' = \mathbf{T}'\mathbf{B}_e^{-1}. \tag{38}$$

Therefore, for pure shear (38) yields the equivalent expressions

$$(\mathbf{B}_e^{-1})_{11} = (\mathbf{B}_e^{-1})_{22}, \qquad b^2 a_p^2 = a^2[b_p^2 + a_p^2\gamma_e^2], \tag{39a, b}$$

where (34) has been used to obtain (39b).

On the other hand, for simple shear the quantities a, b, c are specified by

$$a = b = c = 1, \tag{40}$$

and the stresses $T'_{11}, T'_{22}, T'_{33}, T'_{12}$ and p are determined as functions of γ_e, a_p, b_p.

It is also of interest to note that for either pure or simple shear and small elastic distortions the quantities a, b, c, a_p, b_p are either unity or differ from unity by second order quantities so that with the help of (19), (23), (30c) and (34) the shearing component of Cauchy stress may be approximated by

$$T_{12} = T'_{12} \approx \mu_0\gamma_e. \tag{41}$$

5. FIRST ORDER MATERIAL CONSTANTS

In this section we determine values for the material constants that characterize the first order elastic-viscoplastic response of OFE copper and 70:30 α brass. Although a procedure has been developed by Chan *et al.* (1988) to determine the material constants when m_1 is constant, their procedure does not apply directly when m_1 is taken to be a function of κ (see 18) as is done here.

For convenience, in all of the following figures we identify experimental data with open circles. Figures 2(a, b) show the theoretical predictions together with the experimental results of Kocks *et al.* (1989, Fig. 1) for a large deformation torsion of copper and brass, respectively, and Fig. 2(c) shows the theoretical predictions together with the experimental results of Corten and Elsesser (1952) for brass subjected to small deformation cyclic loading in simple tension. In these figures the effective stress σ_e is defined by (13) and the effective total strain ε_e is defined by (B2). The material constants used for these simulations are listed in Tables 1 and 2 and C_μ, C_2 are specified by

$$C_\mu = 0, \qquad C_2 = 0. \tag{42a, b}$$

Details of the determination of these material constants will be described in this section and the next. Furthermore, Kocks *et al.* (1989, Fig. 1) showed that texture effects cause the curves of effective stress σ_e versus effective total strain ε_e to be different for large deformation tension, compression and torsion experiments. However, the model described in the previous sections does not include texture effects so these differences cannot be modelled. Consequently, since we are mainly interested in second order effects in torsion we have chosen the torsion curves in Figs 2(a, b) for determining the material constants.

Representative values for the first order elastic constants (1a) were obtained: for copper using the formula (7b) and data from Swegle and Grady (1985); and for brass using data from Malvern (1969); these values are recorded in Table 1.

The procedure for determining values for the constants

$$\{\Gamma_0, n\}, \qquad \{\kappa_0, Z_1, Z_3, ma, mb, mc, m_2\}, \tag{43a, b}$$

that characterize the viscoplastic response and hardening of the material is more involved and is considered next. In general the value of n controls the strain-rate sensitivity of the material, with high sensitivity for low values of n and low sensitivity for high values of n. The value of $n = 7.5$ for copper is obtained from Bodner (1987) and indicates that copper is relatively strain-rate insensitive up to moderate values of strain rate ($< 10^3\,s^{-1}$). Although

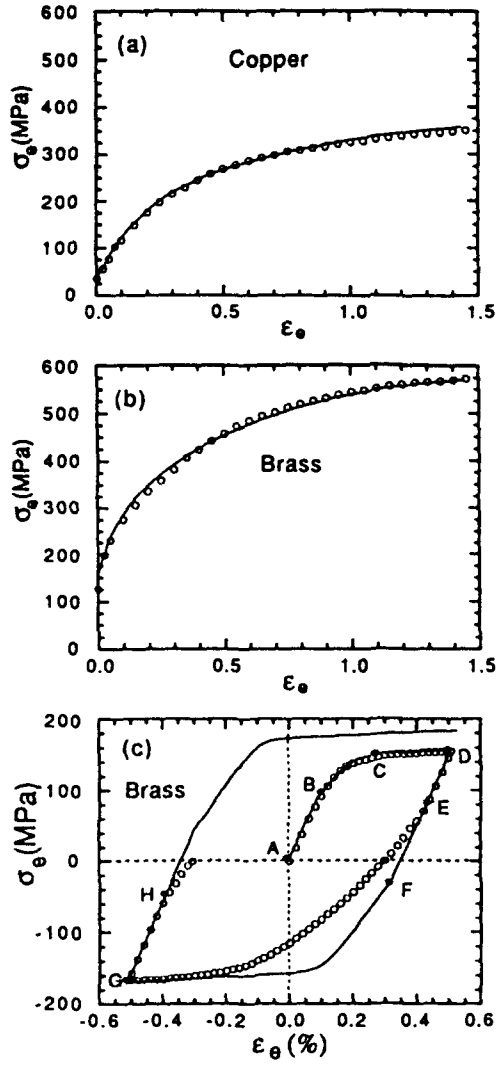

Fig. 2. First order response: simulations and experiments.

Table 1. First order elastic constants

	K_0 (GPa)	μ_0 (GPa)
OFE Copper	138.10	47.70
70:30 α Brass	96.90	36.43

Table 2. First order viscoplastic and hardening constants

	OFE Copper	70:30 α Brass
Γ_0 (s^{-1})	10^7	10^7
n	7.5	7.5
κ_0 (GPa)	0.044	0.108
Z_1 (GPa)	0.52	0.675
Z_3 (GPa)	0.0	0.078
ma (GPa^{-1})	55.1	37.8
mb (GPa^{-1})	2.21	3.33
mc (GPa^{-1})	9.3	10.1
m_2 (GPa^{-1})	0.0	25,000.0

no value of n for brass was found in the literature we specified $n = 7.5$ because brass is also known to be relatively rate insensitive (Kleemola and Ranta-Eskola, 1979) up to moderate values of strain rate. In any case, since here we are not focusing on the strain-rate sensitivity of the material response, the specific value of n is relatively unimportant. Furthermore, we note that the value of Γ_0 mainly controls the strain-rate sensitivity in the high strain-rate region ($>10^5\ s^{-1}$). Also, the response of reasonably strain-rate insensitive materials is relatively insensitive to the value of Γ_0 up to moderate strain rates. Consequently, we arbitrarily specified $\Gamma_0 = 10^7\ s^{-1}$.

The remaining constants (43b) control hardening and are determined by an iterative procedure used to match experimental stress–strain curves. This procedure will first be described for brass because it includes the Bauschinger effect and therefore is representative of the most general material described by the proposed constitutive equations.

To determine the first order response associated with the torsion experiments of Kocks *et al.* (1989) it is sufficient to consider simple shear and use (29), (40), (B1) and (B2) to deduce that the equivalent total strain rate $\dot{\varepsilon}_e$ becomes

$$\dot{\varepsilon}_e^* = |\dot{\gamma}^*|/\sqrt{3}, \tag{44}$$

where, for convenience, throughout the rest of the text we use a superposed (*) to denote values associated with experiments. Similarly, for simple tension it is sufficient to approximate the deformation as isochoric [$b = 1/\sqrt{a}$ in (C1) of Appendix C] and use (B1), (B2) and (C1) to deduce that

$$\dot{\varepsilon}_e^* \approx |\dot{a}^*|/a^*, \tag{45}$$

where a^* denotes the experimental value of a. It follows with the help of (12) and the approximations (B6) and (B9) that an estimate Z^* of the value of Z for points on a stress–strain curve with a significant plastic deformation rate can be obtained by the formula

$$Z^* \approx \sigma_e^* \left[2 \ln \left\{ \frac{\sigma_e^* \Gamma_0}{3\mu \dot{\varepsilon}_e^*} \right\} \right]^{1/2n}, \tag{46}$$

where σ_e^* is the experimental value of the effective stress σ_e. In particular, since the curves in Figs 2(a, b) represent loading only, the quantity Z^* can be expressed as a function of ε_e^*.

The work of Chan *et al.* (1988) suggests that for many materials the directional hardening saturates much faster (smaller levels of plastic strain) than the isotropic hardening. This suggests that the hardening exhibited in the region BC in Fig. 2(c) is mainly due to directional hardening so that the value of Z_B^* of Z^* at point B and the value Z_C^* of Z^* at point C in Fig. 2(c) can be used to estimate the initial value κ_0 of isotropic hardening and the saturated value Z_3 of directional hardening by the formulae

$$\kappa_0 \approx Z_B^*, \qquad Z_3 \approx Z_C^* - Z_B^*. \tag{47a, b}$$

Once an estimate of Z_3 is specified, approximate values κ^* of κ can be determined for the large deformation torsion experiment in Fig. 2(b) by using (46) and the formula

$$\kappa^* \approx Z^* - Z_3, \tag{48}$$

which assumes that directional hardening has saturated. This formula is used for the region in which κ^* is greater than or equal to the value κ_0 given by (47a). Then approximate values $m_1^*(\kappa^*)$ of the function $m_1(\kappa)$ in (16a) and (18) can be determined by assuming a value for Z_1 and using (16a), (48) and (B10) with $I_3 \approx 1$ to obtain

$$m_1^*(\kappa^*) \approx \frac{\dot{Z}^*}{(Z_1 - \kappa^*)\sigma_e^* \dot{\varepsilon}_e^*}, \qquad \dot{Z}^* \approx \frac{dZ^*}{d\varepsilon_e^*}\dot{\varepsilon}_e^*, \tag{49a, b}$$

where (49b) can be obtained by numerically differentiating the curve $Z^*(\varepsilon_e^*)$ obtained from (46) and the experimental data. Values for the constants ma, mb, mc are obtained by requiring the function (18) to approximate the result (49a). Finally, a value for m_2 in (16b) is determined by attempting to match the small strain response in region BC of Fig. 2(c).

It is important to note that even the large deformation torsion experiments in Figs 2(a, b) do not predict a saturated value of flow stress so they do not provide a definite measure of the value of Z_1. For our purposes we specified the value of Z_1 by extrapolating the curves of Z^* associated with these experiments.

Once estimates of the first order material constants have been determined it is possible to simulate the experiments by calculating the response to simple shear and cyclic simple tension using the nonlinear constitutive equations of the previous sections and assuming that

$$\dot{\varepsilon}_e = \frac{1}{\sqrt{3}} \times 10^{-3}\,s^{-1}, \tag{50}$$

for the experiments. In this regard we recall that since the materials under consideration are relatively strain-rate insensitive the predictions will be reasonably unaffected if the value of $\dot{\varepsilon}_e$ is varied even by plus or minus an order of magnitude. Consistent with (44) and (50) we specified

$$\dot{\gamma} = 10^{-3}\,s^{-1}, \tag{51}$$

in simulating simple shear and used eqns (30), (33), (34), (40), and the material constants in Tables 1, 2 and in (42) to solve the flow rule (11) for a_p, b_p, γ_p and obtain the stress from (20). Also, consistent with (50) and the small deformation approximation of (45) [$a^* \approx 1$] we specified

$$\dot{a} = \pm \frac{1}{\sqrt{3}} \times 10^{-3}\,s^{-1}, \tag{52}$$

in simulating simple tension, where the sign of $\dot{a}$ changes abruptly at the points D and G in Fig. 2(c) associated with load reversal. Next we used the eqns (C1), (C3), (C4) in Appendix C, and the material constants in Tables 1, 2 and in (42) to solve the condition (C2) for b and the flow rule (11) for a_p, b_p. Then a value for the stress T_{11} was obtained from (20). Based on the results of these simulations the values of κ_0, m_2, Z_3 were slightly adjusted to obtain better comparison with the experimental data.

The procedure for obtaining the material parameters for copper is simpler than that for brass because copper does not exhibit a pronounced Bauschinger effect so m_2 and Z_3 vanish and we do not attempt to match experimental data for cyclic simple tension.

The final values of the material constants obtained by this iterative procedure are summarized in Table 2 and the theoretical predictions (Case I) are compared with the experimental data in Figs 2(a, b, c). These figures suggest that the model simulates the large deformation torsion experiments quite well but that it can only simulate the main features of the cyclic simple tension experiment on brass. This is because the model necessarily predicts that the plastic response during unloading and reloading [curve DEFG in Fig. 2(c)] cannot occur until the stress has crossed the zero axis, whereas the experiment indicates that plastic response begins at point E in Fig. 2(c). However, the yielding at points E and H shown in Fig. 2(c) is generally observed to be a transient effect that persists only for a few cycles. Consequently, we expect this transient effect to be negligible on the prediction of the Freudenthal–Ronay effect, which is associated with a large number of cycles.

Table 3. Second order elastic constants

	OFE Copper	70:30 α Brass
s_1	1.41	1.41
m_p [TPa^{-1}]	28.0	28.0
C_2	22.5	2.42

Table 4. Definition of Cases I–IV

Case	C_2	C_μ
I	0	0
II	Table 3	0
III	0	1
IV	Table 3	1

6. SECOND ORDER MATERIAL CONSTANTS

It remains to determine values for the second order constants (1b). To this end we note that values for the constants s_1 and m_p can be obtained by analysing data from plate impact shock experiments. In particular for copper, a value of s_1 is recorded by Pugh (1970) and a value for m_p can be obtained from the work by Steinberg *et al.* (1980) (note that $m_p = \mu_p/\mu_0$ in their notation). Values of these constants were not found in the literature for 70:30 α brass so for the simulations here we assumed them to be the same as those for copper. These values are summarized in Table 3.

As mentioned in the introduction, a value for the elastic constant C_2 was determined by matching the value of axial elongation measured during torsion into the plastic region instead of matching results of a purely elastic experiment. To this end, we simulated pure shear with a shearing rate specified by (51), using eqns (30), (33), (34) and the material constants for copper in Tables 1, 2, 3 and Case IV in Table 4, and the values

$$C_2 = \{-4, -2, 0, 4, 8, 12, \ldots, 36\}. \tag{53}$$

Then we solved the conditions (36a, b) and (39b) for a, b, c; the flow rule (11) for a_p, b_p, γ_p; and (20) for the component T_{12} of stress.

For convenience in presenting these results we define the elongations E_1, E_2, E_3 by the formulae

$$E_1 = a - 1, \qquad E_2 = b - 1, \qquad E_3 = c - 1. \tag{54a, b, c}$$

Figure 3 shows that the axial elongation E_2 at a given value of shear γ is a linear function of the value of C_2. It is of particular interest to note that axial elongation vanishes for any

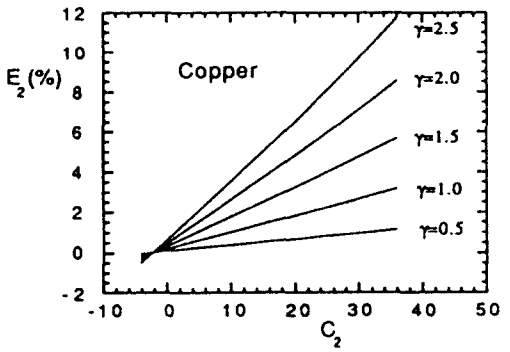

Fig. 3. Axial elongation versus the material constant C_2 for copper.

value of shear γ when the value of $C_2 \approx -2$ (see Appendix D). Assuming that all the lines in Fig. 3 pass through $C_2 = -2$, it is easy to determine the value of C_2 required to match experimental data for axial elongation E_2 at a given value of shear γ by doing a single simulation of pure shear with $C_2 \neq -2$ to obtain a second point on the line for the given value of γ. Using this procedure we obtained the values of C_2 given in Table 3.

Figures 4(a, b) show the theoretical predictions using these values of C_2 together with the experimental data for copper and brass (Swift, 1947). These results indicate that texture effects do not influence axial elongation until large deformations even though these texture effects probably begin (Kocks *et al.*, 1989; Harren *et al.*, 1989) before the theoretical and experimental curves diverge.

7. ADDITIONAL SIMULATIONS

Having determined values for all the material constants (summarized in Tables 1, 2, 3) it is of interest to examine theoretical predictions for pure shear, simple shear and the accumulated axial elongation caused by cyclic pure shear. Also, for pure and simple shear we will examine the specific influence of the dependence of the Helmholtz free energy on the measure β_2 of distortional deformation by comparing with the results for $C_2 = 0$, and the influence of the dependence of the shear modulus μ on dilatation I_3 by comparing with the results for $C_\mu = 0$. To this end we define Cases I, II, III, IV in Table 4.

Figure 5 shows the predictions of pure shear and Fig. 6 shows the predictions of simple shear. Firstly, we note from Figs 5(a, c) and Figs 6(a, c) that the first order response is nearly identical for all of these Cases, which means that each of these Cases matches the experimental data in Figs 2(a, b). Furthermore, these results justify our earlier statement that the material constants that characterize first order response can be determined independently of those that characterize second order response. For pure shear it appears that the second order response is mainly controlled by the constant C_2 and is nearly unaffected by the value of C_μ because the predictions of Cases I and III are nearly equal and the predictions of Cases II and IV are nearly equal whereas the predictions of Cases I and II are quite different. Using the approximations (31) and the definitions (54) it follows from

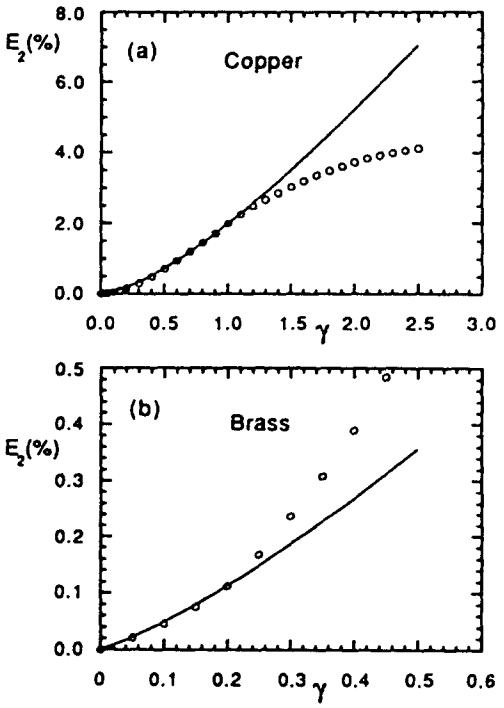

Fig. 4. Axial elongation: simulations and experiments.

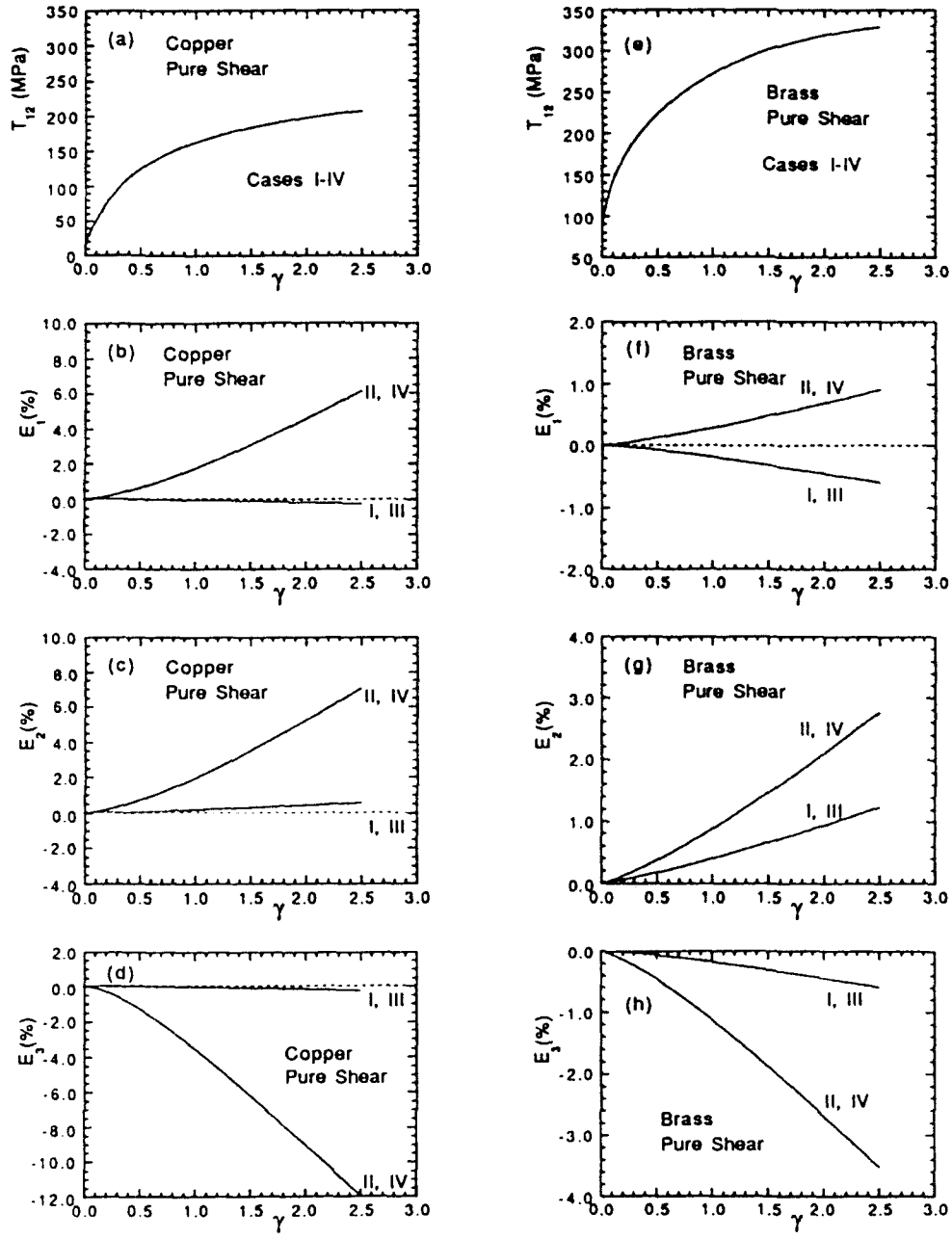

Fig. 5. Simulations of pure shear.

Fig. 5 that a hollow tube of copper or brass subjected to pure torsion would be predicted (Case IV) to increase in length, increase in mean radius and decrease in thickness, maintaining nearly constant volume.

Figure 6 shows that for simple shear the magnitudes of the normal stresses are influenced by both the constants C_2 and C_μ. However, by comparing Figs 6(b, c, d) with Figs 6(f, g, h) we may conclude that the value of C_2 has a strong effect on the normal stresses because from Table 3 the value of C_2 is large for copper and small for brass. Also, note from Fig. 6 that the normal stresses are about an order of magnitude smaller than the shear stress, which is consistent with experiments. For example, the maximum value of normal compressive stress ($-T_{22}$) in Fig. 6(c) for copper is about 15 MPa which compares to 25 MPa reported by Montheillet *et al.* (1984, in their Fig. 5, where compression is plotted as positive).

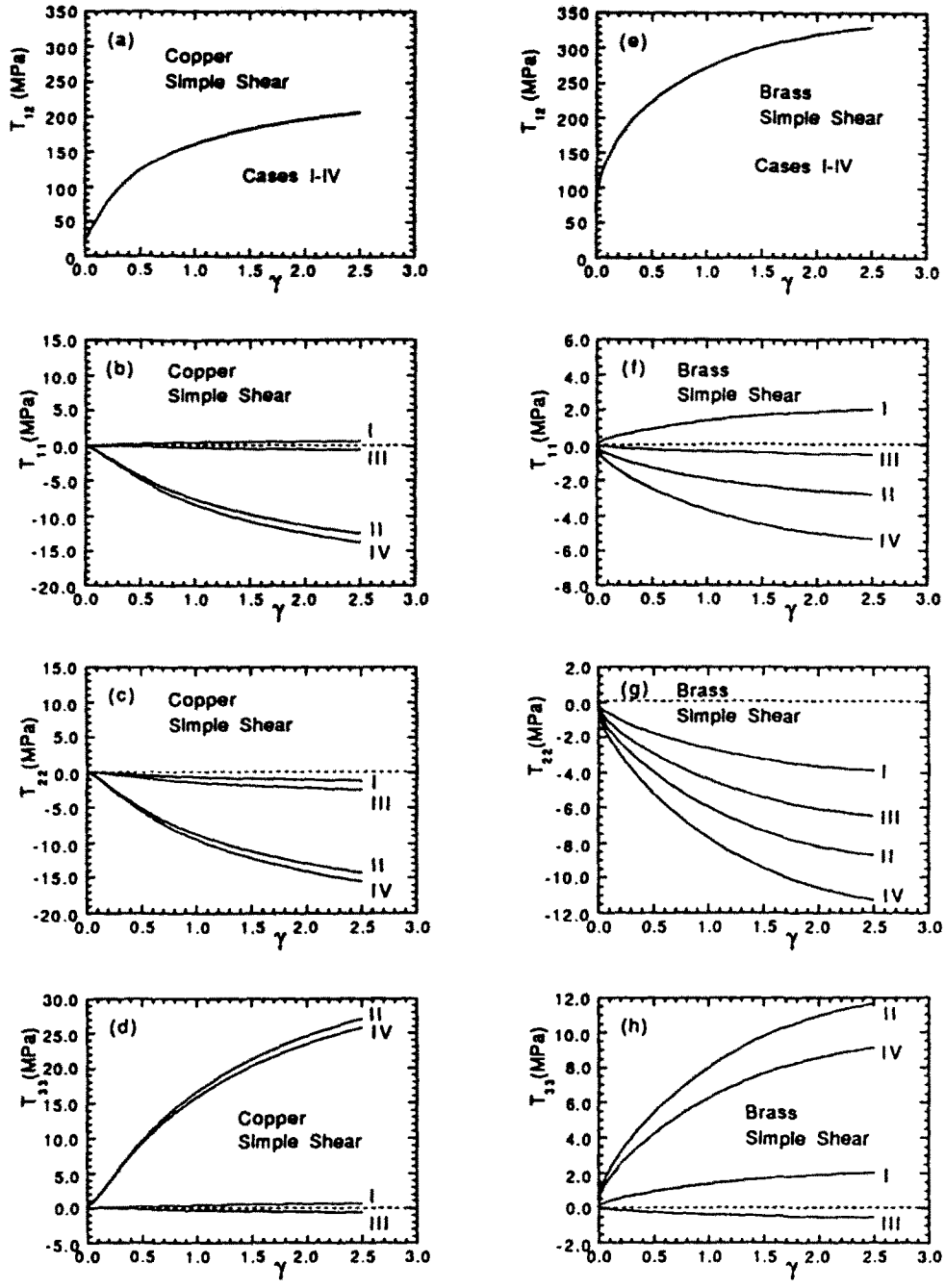

Fig. 6. Simulations of simple shear.

Swift (1947) also observed for torsion without axial constraint that upon load reversal the axial elongation decreases slightly and then continues to increase with a net increase in length. Figure 7 shows the shear stress and axial elongation for pure shear in copper with the shearing rate specified by

$$\dot{\gamma} = \pm 10^{-3}\,\mathrm{s}^{-1}, \tag{55}$$

where the sign of $\dot{\gamma}$ changes abruptly at points of load reversal. Curve ABC is associated with no load reversal and curve ABDEF shows the response with load reversal. The portion of the curve DF in Fig. 7b indicates no significant decrease in axial elongation upon load reversal. This again indicates a limitation of the present theory which does not model texture

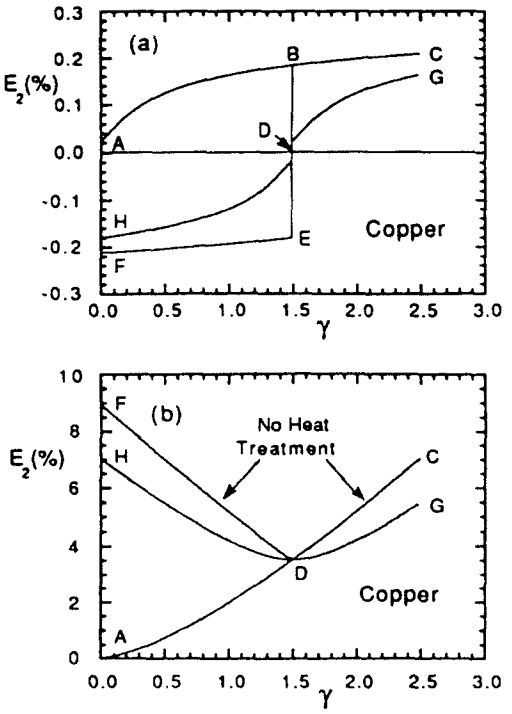

Fig. 7. Effects of simulated heat treatment for various loading paths.

effects because it was shown by Harren *et al.* (1989) that the decrease in axial elongation during the load reversal observed by Swift (1947) is mainly due to texture effects.

Further in this regard Swift (1947) showed that the decrease in axial elongation upon load reversal disappeared when the material was annealed at zero stress before application of the load reversal. To simulate this effect we unloaded the material from point B to D in Fig. 7 and then reset the value of isotropic hardening κ to its initial value κ_0. This simulates the effect of including thermal recovery of hardening associated with the annealing process. Then the loading was continued along either the path DG or DH. Figure 7(b) shows that the shape of the axial elongation curve after annealing is very similar to the initial portion of the curve AD, which qualitatively is the same result observed by Swift (1947).

Next, we consider the Freudenthal–Ronay effect of accumulated axial elongation during small amplitude cyclic torsion with no axial load. Although Freudenthal and Ronay (1966) performed their experiments on aluminium we cannot match their experiments directly because we do not have enough experimental data to determine all the material parameters for aluminium. On the other hand, our material constants for brass have been verified more than those for copper because they have been determined to match experimental data for cyclic simple tension [Fig. 2(c)] in addition to large torsion [Fig. 2(b)] and the Swift effect [Fig. 4(b)]. Furthermore we recall that the only hollow tube used by Swift was made of brass. Consequently, we have decided to simulate the Freudenthal–Ronay effect on brass even though experimental data for this effect are not available.

For these simulations we specify the shearing rate by (55). Figure 8 shows the shear stress and axial elongation as functions of shear γ for two amplitudes ($\gamma = \pm 0.01$ and $\gamma = \pm 0.03$). From Fig. 8(b) we observe that upon load reversal the axial elongation decreases slightly due to elastic recovery and then continues to increase with a net increase in length dependent on the amplitude of the cycle. This decrease in axial elongation due to elastic recovery should not be confused with the observations of Swift (1947) which persisted well into the plastic region during reverse loading.

To further examine the influence of amplitude of a cycle and the number of cycles on axial elongation, let $\bar{E}_2$ be the accumulated axial elongation at the end of any number of cycles. Figures 9(a, b) show curves of $\bar{E}_2$ as functions of the number of cycles for different

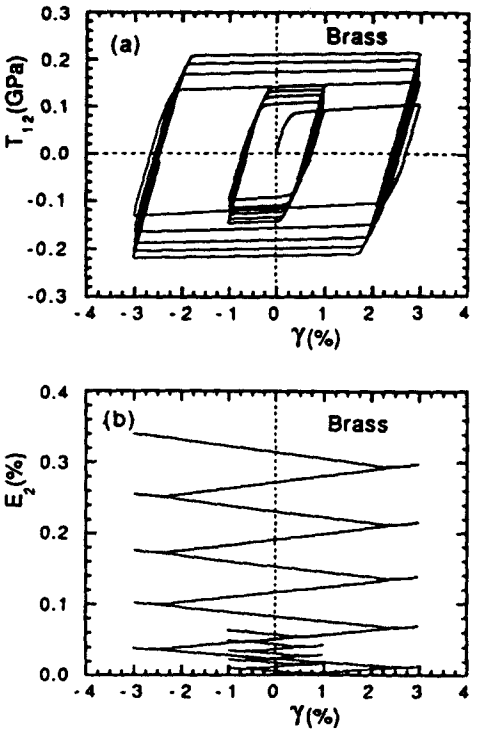

Fig. 8. Simulations of cyclic loading: (a) stress–strain; (b) axial elongation.

amplitudes of the cycle, and Fig. 9(c) shows curves of $\bar{E}_2$ as functions of the amplitude of the cycle for different numbers of cycles. The values of the amplitude A in degrees marked in Figs 9 and 10 are determined by the relative twist between the ends of the torsion specimens in the experiments of Freudenthal and Ronay (1966) and may be related to the amplitude of shear γ by the formula

$$\gamma = \pm A \text{ (deg)} \times 1.53 \times 10^{-3} \text{ (rad/deg)}. \tag{56}$$

In particular, note from Fig. 9(a) that if the amplitude is small enough then the accumulated axial elongation $\bar{E}_2$ saturates when the value of isotropic hardening increases to the point that the cycle remains elastic. In contrast, if the amplitude is large enough then a portion of the cycle will remain plastic and $\bar{E}_2$ will continue to increase. Also note from Fig. 9(c) that when the amplitude is large enough the cycle is nearly all plastic and $\bar{E}_2$ is nearly a linear function of the number of cycles. Furthermore, we note that our predictions for brass in Fig. 9(a) seem reasonable because they are qualitatively and quantitatively similar to the experimental data for aluminium reported in Fig. 10(d) of Freudenthal and Ronay (1966).

From the experimental results of Swift (1947, Figs 10, 12) one observes that during reverse loading the axial elongation decreases even during plastic response. This same effect was observed by Harren *et al.* (1989) and attributed to texture development. Consequently, it is expected that texture development will tend to decrease the magnitude of accumulated axial elongation during cyclic torsional loading relative to the magnitudes predicted in Fig. 9.

To demonstrate a connection between the accumulated axial elongation during cyclic loading and axial elongation during monotonic loading we use (33) and the fact that a_p remains nearly equal to one to approximate the accumulated plastic shear by

$$\bar{\gamma}_p = \int_0^t |\dot{C}_{p12}| \, dt. \tag{57}$$

Figure 10 shows curves of $\bar{E}_2$ versus $\bar{\gamma}_p$ for monotonic loading (line with squares) and for

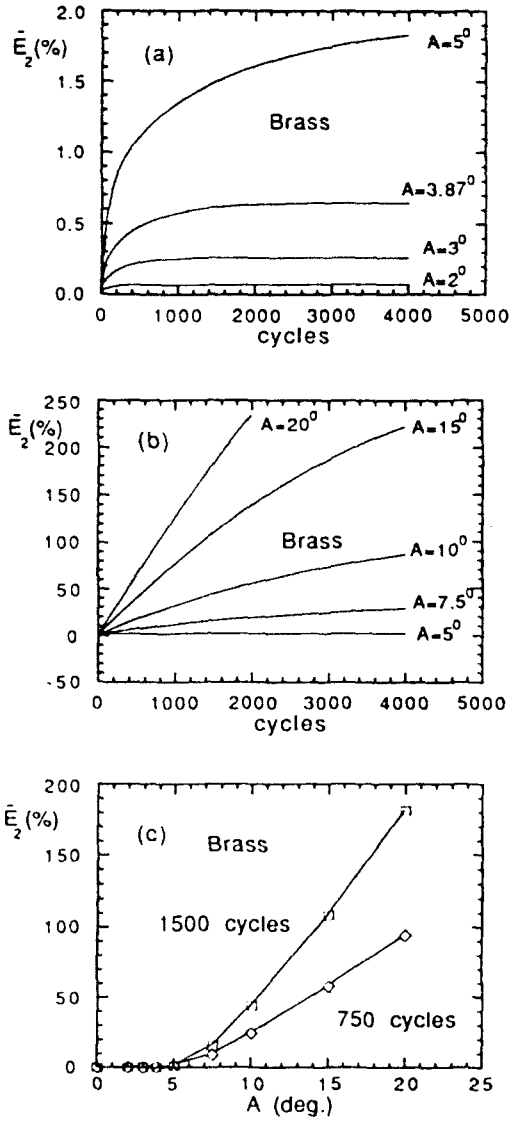

Fig. 9. Simulation of accumulated axial elongation : (a) and (b) for different angles of twist A; (c) for different numbers of cycles.

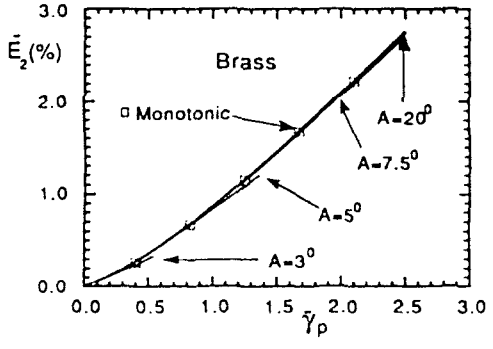

Fig. 10. Accumulated axial elongation for monotonic and cyclic loading versus accumulated plastic shear strain $\bar{\gamma}_p$ [see eqn (7.3)].

four different amplitudes of twist ($A = \pm 3°, 5°, 7.5°, 20°$). This figure shows clearly that the accumulated axial elongation $\bar{E}_z$ depends mainly on the accumulated plastic shear $\bar{\gamma}_p$. In view of the results in Fig. 4(b) and Fig. 10 we may conclude that texture effects become significant for accumulated plastic strains greater than about $\bar{\gamma}_p = 0.2$, which indicates that the predictions in Fig. 9(b) for large angles of twist are exaggerated.

Since the calculation based on the nonlinear theory requires considerable numerical effort to iteratively solve the conditions (36a, b) and (39b) for a, b, c for each time step, calculation of the accumulated axial elongation for many cycles can be quite costly. However, the result shown in Fig. 10 suggests that it is possible to estimate the value of $\bar{E}_z$ for a given number of cycles by estimating the value of $\bar{\gamma}_p$ and determining $\bar{E}_z$ from the curve for monotonic loading. This procedure can cause considerable simplification if the value of $\bar{\gamma}_p$ is estimated by simulating the cyclic loading using the linear theory for which the nontrivial components of the stress are given by (41), the flow rule (11) and evolution equation of hardening (16b) are given by

$$\dot{\bar{\gamma}}_p = \Gamma(\gamma - \bar{\gamma}_p), \qquad \dot{\beta}_{12} = m_2(\rho_0\theta\xi')(Z_3 \operatorname{sign}\{T_{12}\} - \beta_{12}), \tag{58a, b}$$

where with the help of (28), (B6) and the condition $I_3 \approx 1$, the rate of plastic dissipation becomes

$$\rho_0\theta\xi' = \frac{\Gamma\sigma_e^2}{3\mu}. \tag{59}$$

8. CONCLUSION

Nonlinear constitutive equations for an elastically isotropic elastic-viscoplastic material have been used to predict the second order effects that cause: axial elongation during pure shear, normal stresses during simple shear, and accumulated axial elongation during cyclic pure shear. Specific attention has been focused on the determination of the material constants for OFE copper and 70:30 α brass. It has been shown that these constitutive equations have the simplifying feature that the constants controlling the first order response can be determined independently of those controlling the second order response. In particular the rate of hardening was modified to obtain agreement with experimental data for large deformation torsion. Although texture effects are significant for large deformations, the results of this paper indicate that second order effects in the plastic region are driven by second order elastic effects that cause small terms to appear in the flow rule which continue to influence the accumulation of plastic deformation. Specifically, the value of the second order elastic constant C_2, which controls these second order effects, can be determined by matching experimental data for axial elongation during torsion without axial constraint.

REFERENCES

Bodner, S. R. (1985). Evolution equations for anisotropic hardening and damage of elastic-viscoplastic materials. In *Plasticity Today—Modelling, Methods and Applications* (Edited by A. Sawczuk and G. Bianchi), pp. 471-482. Elsevier, London.

Bodner, S. R. (1987). Review of a unified elastic-viscoplastic theory. In *Equations for Creep and Plasticity* (Edited by A. K. Miller), pp. 273-301. Elsevier, Oxford.

Bodner, S. R. and Partom, Y. (1972). A large deformation elastic-viscoplastic analysis of a thick-walled spherical shell. *J. Appl. Mech.* **39**, 751-757.

Bodner, S. R. and Partom, Y. (1975). Constitutive equations for elastic-viscoplastic strain-hardening materials. *J. Appl. Mech.* **42**, 385-389.

Chan, K. S., Bodner, S. R. and Lindholm, U. S. (1988). Phenomenological modeling of hardening and thermal recovery in metals. *J. Engng Mater. Tech.* **110**, 1-8.

Chen, R. (1990). Second order effects in elastic-viscoplastic materials subjected to finite shear strain. Masters Thesis (in Hebrew), Technion—Israel Institute of Technology, Haifa, Israel.

Corten, H. T. and Elsesser, T. M. (1952). The effect of slightly elevated-temperature treatment upon microscopic and submicroscopic residual stresses induced by small elastic strains. *Trans. ASME* **74**, 1297-1302.

Flory, P. J. (1961). Thermodynamic relations for high elastic materials. *Trans. Faraday Soc.* **57**, 829-838.

Freudenthal, A. M. and Ronay, M. (1966). Second order effects in dissipative media. *Proc. R. Soc.* **A292**, 14-50.

Green, A. E. and Naghdi, P. M. (1965). A general theory of an elastic-plastic continuum. *Archiv. Rational Mech. Anal.* **18**, 251–281.
Green, A. E. and Naghdi, P. M. (1966). A thermodynamic development of elastic-plastic continua. Proceedings of the IUTAM Symposia, Vienna (Edited by H. Parkus and L. I. Sedov), pp. 117–131.
Green, A. E. and Naghdi, P. M. (1977). On thermodynamics and the nature of the second law. *Proc. R. Soc. Lond.* **A357**, 253–270.
Green, A. E. and Naghdi, P. M. (1978). The second law of thermodynamics and cyclic processes. *J. Appl. Mech.* **45**, 487–492.
Harren, S., Lowe, T. C., Asaro, R. J. and Needleman, A. (1989). Analysis of large-strain shear in rate-dependent face-centred cubic polycrystals: correlation of micro- and macromechanics. *Phil. Trans. R. Soc. Lond.* **A328**, 443–500.
Im, S. and Atluri, S. N. (1987). A study of two finite strain plasticity models: an internal time theory using Mandel's director concept, and a general isotropic/kinematic-hardening theory. *Int. J. Plasticity* **3**, 163–191.
Kleemola, H. J. and Ranta-Eskola, A. J. (1979). Effect of strain rate and deformation temperature on the strain hardening of sheet steel and brass in uniaxial tension. *Sheet Metal Industries* **48**, 1046–1057.
Kocks, U. F., Stout, M. G. and Rollet, A. D. (1989). The influence of texture on strain hardening. *Strength of Metals and Alloys* (ICSMA 8), Pergamon Press, Oxford. Proceedings of the 8th International Conference on the Strength of Metals and Alloys, Tampere, Finland, 22–26 August 1988, pp. 25–34.
Lipkin, J., Chiesa, M. L. and Bammann, D. J. (1988). Thermal softening of 304L stainless steel: experimental results and numerical simulations. In *Impact Loading and Dynamic Behavior of Materials* (Edited by C. Y. Chiem, H.-D. Kunze and L. W. Meyer), Vol. 2, pp. 687–694. DGM Informationsgesellschaft.
Malvern, L. E. (1969). *Introduction to the Mechanics of Continuous Media*. Prentice-Hall, New Jersey.
Montheillet, F., Cohen, M. and Jonas, J. J. (1984). Axial stresses and texture development during the torsion testing of Al, Cu, and α-Fe. *Acta Metall.* **32**, 2077–2089.
Poynting, J. H. (1909). On pressure perpendicular to the shear planes in finite pure shears and on lengthening of loaded wires when twisted. *Proc. R. Soc.* **A82**, 546–559.
Pugh, H. D. (1970). *Mechanical Behaviour of Metals Under Pressure*. Elsevier, London.
Ronay, M. (1968). Second order elongations of metal tubes in cyclic torsion. *Int. J. Solids Structures*. **4**, 509–516.
Rubin, M. B. (1986). An elastic viscoplastic model for large deformation. *Int. J. Engng Sci.* **24**, 1083–1095.
Rubin, M. B. (1987a). An elastic viscoplastic model for metals subjected to high compression. *J. Appl. Mech.* **25**, 532–538.
Rubin, M. B. (1987b). An elastic viscoplastic model exhibiting continuity of solid and fluid states. *Int. J. Engng Sci.* **25**, 1175–1191.
Rubin, M. B. (1988). The significance of pure measures of distortion in nonlinear elasticity with reference to the Poynting problem. *J. Elasticity* **20**, 53–64.
Rubin, M. B. (1989). A time integration procedure for plastic deformation in elastic viscoplastic metals. *J. Appl. Math. Phys.* (ZAMP) **40**, 846–871.
Rubin, M. B. (1990). Analysis of viscoplasticity in 6061-T6 aluminum. *J. Appl. Phys.* **68**, 4523–4530.
Rubin, M. B. and Chen, R. (1991). Universal relations for elastically isotropic elastic plastic materials. *J. Appl. Mech.* **58**, 283–285.
Steinberg, D. J., Cochran, S. G. and Guinan, M. W. (1980). A constitutive model for metals applicable at high strain rate. *J. Appl. Phys.* **51**, 1498–1504.
Swegle, J. W. and Grady, D. E. (1985). Shock viscosity and the prediction of shock wave rise times. *J. Appl. Phys.* **58**, 692–701.
Swift, H. W. (1947). Length change in metals under torsional overstrain. *Engineering* **163**, 253–257.

APPENDIX A

In this appendix we record some formulae which are useful in developing approximate expressions for small elastic distortion. First we use (19c, d) to obtain an expression for $\mathbf{g}_e' \cdot \mathbf{I}$ by noting that

$$-1 = \det(-\mathbf{B}_e') = \det(2\mathbf{g}_e' - \mathbf{I}) = -1 + 2\mathbf{g}_e' \cdot \mathbf{I} - \tfrac{1}{2}[(2\mathbf{g}_e' \cdot \mathbf{I})^2 - (2\mathbf{g}_e' \cdot 2\mathbf{g}_e')] + \det(2\mathbf{g}_e'). \tag{A1}$$

Solving (A1) for $\mathbf{g}_e' \cdot \mathbf{I}$ we deduce that

$$\mathbf{g}_e' \cdot \mathbf{I} = \tfrac{1}{2}[1 - \sqrt{1 + 4(\mathbf{g}_e' \cdot \mathbf{g}_e' + 4 \det \mathbf{g}_e')}], \tag{A2}$$

where the minus sign is used to obtain the correct limit as $\mathbf{g}_e'$ approaches zero. Thus, for small elastic distortion (A2) may be approximated by

$$\mathbf{g}_e' \cdot \mathbf{I} \approx -\mathbf{g}_e' \cdot \mathbf{g}_e'. \tag{A3}$$

Next with the help of the Cayley–Hamilton theorem we write

$$-\mathbf{B}_e'^{-1} + (\mathbf{B}_e'^{-1} \cdot \mathbf{I})\mathbf{B}_e'^{-2} - \tfrac{1}{2}[(\mathbf{B}_e'^{-1} \cdot \mathbf{I})^2 - (\mathbf{B}_e'^{-1} \cdot \mathbf{B}_e'^{-1})]\mathbf{B}_e'^{-1} + \mathbf{I} = 0. \tag{A4}$$

Now taking the inner product of (A4) with $\mathbf{B}_e'$ we deduce that

$$\mathbf{B}_e' \cdot \mathbf{I} = \tfrac{1}{2}[(\mathbf{B}_e'^{-1} \cdot \mathbf{I})^2 - (\mathbf{B}_e'^{-1} \cdot \mathbf{B}_e'^{-1})]. \tag{A5}$$

However, from (19d) we have

$$\mathbf{B}_e'^{-1}\cdot\mathbf{I} = 3-2\mathbf{g}_e'\cdot\mathbf{I}, \qquad \mathbf{B}_e'^{-1}\cdot\mathbf{B}_e'^{-1} = 3-4\mathbf{g}_e'\cdot\mathbf{I}+4\mathbf{g}_e'\cdot\mathbf{g}_e'. \tag{A6}$$

so the expression (A5) may be rewritten in the form

$$\mathbf{B}_e'\cdot\mathbf{I} = \tfrac{1}{2}[6-8\mathbf{g}_e'\cdot\mathbf{I}+4(\mathbf{g}_e'\cdot\mathbf{I})^2-4(\mathbf{g}_e'\cdot\mathbf{g}_e')]. \tag{A7}$$

Similarly, taking the inner product of (A4) with $\mathbf{B}_e'^2$ and using (A5) it may be shown that

$$\mathbf{B}_e'^2\cdot\mathbf{I} = -2(\mathbf{B}_e'^{-1}\cdot\mathbf{I})+\tfrac{1}{2}[(\mathbf{B}_e'^{-1}\cdot\mathbf{I})^2-(\mathbf{B}_e'^{-1}\cdot\mathbf{B}_e'^{-1})]^2. \tag{A8}$$

Consequently, with the help of (A3), (A6), (A7) and (A8) it can be shown that for small elastic distortion

$$\mathbf{B}_e'\cdot\mathbf{I} \approx 3[1+\tfrac{2}{3}(\mathbf{g}_e'\cdot\mathbf{g}_e')], \qquad \frac{3}{\mathbf{B}_e'\cdot\mathbf{I}} \approx [1-\tfrac{2}{3}(\mathbf{g}_e'\cdot\mathbf{g}_e')], \qquad \mathbf{B}_e'^2\cdot\mathbf{I} \approx 3+8(\mathbf{g}_e'\cdot\mathbf{g}_e'). \tag{A9a, b, c}$$

APPENDIX B

With the help of (3c), (22) and (27) the deviatoric part $\mathbf{D}'$ of the symmetric part $\mathbf{D}$ of the velocity gradient $\mathbf{L} = \dot{\mathbf{F}}\mathbf{F}^{-1}$ is defined such that

$$\mathbf{D} = \tfrac{1}{2}(\mathbf{L}+\mathbf{L}^{\mathrm{T}}), \qquad \mathbf{D}' = \mathbf{D}-\tfrac{1}{3}(\mathbf{D}\cdot\mathbf{I})\mathbf{I} = \tfrac{1}{2}(\mathbf{F}'^{-\mathrm{T}}\dot{\mathbf{C}}'\mathbf{F}'^{-1}). \tag{B1a, b}$$

It follows that the equivalent total strain rate $\dot{\varepsilon}_e$ which is defined by

$$\dot{\varepsilon}_e = (\tfrac{2}{3}\mathbf{D}'\cdot\mathbf{D}')^{1/2}, \tag{B2}$$

may be rewritten in the form

$$\dot{\varepsilon}_e = (\tfrac{1}{4}\mathbf{C}'^{-1}\dot{\mathbf{C}}'\cdot\dot{\mathbf{C}}'\mathbf{C}'^{-1})^{1/2}. \tag{B3}$$

By analogy we define the equivalent plastic strain rate $\dot{\varepsilon}_p$ by

$$\dot{\varepsilon}_p = (\tfrac{1}{4}\mathbf{C}_p^{-1}\dot{\mathbf{C}}_p\cdot\dot{\mathbf{C}}_p\mathbf{C}_p^{-1})^{1/2}, \tag{B4}$$

where we have used the fact that $\mathbf{C}_p$ is a pure measure of plastic distortion since it is unimodular (3d). Substituting the flow rule (11) into (B4) and using the definitions (19) it follows that

$$\dot{\varepsilon}_p = \Gamma\left[\frac{1}{6}\left\{\left(\frac{3}{\mathbf{B}_e'\cdot\mathbf{I}}\right)^2(\mathbf{B}_e'\cdot\mathbf{B}_e')-3\right\}\right]^{1/2}. \tag{B5}$$

Consequently, for small elastic distortions the approximations (23), (A9) and the definition (13) may be used to deduce that

$$\dot{\varepsilon}_p \approx \Gamma[\tfrac{2}{3}\mathbf{g}_e'\cdot\mathbf{g}_e']^{1/2} \approx \frac{\Gamma\sigma_e}{3\mu}. \tag{B6}$$

Furthermore, it follows from (11), (19), (23) and (A9b) that for small elastic distortion

$$\tfrac{1}{2}\mathbf{F}'^{-\mathrm{T}}\dot{\mathbf{C}}_p\mathbf{F}'^{-1} = \tfrac{1}{2}\Gamma\left[\left(\frac{3}{\mathbf{B}_e'\cdot\mathbf{I}}\right)\mathbf{I}-\mathbf{B}_e'^{-1}\right] \approx \Gamma\mathbf{g}_e' \approx \left(\frac{\Gamma}{2\mu}\right)\mathbf{T}'. \tag{B7}$$

Also, when the stress rate $\dot{\sigma}_e$ is significantly influenced by plastic deformation rate it follows from (21b) that for small elastic distortion

$$\dot{\mathbf{C}}_p = \dot{\mathbf{C}}'+O(\varepsilon), \tag{B8}$$

so that (B3) and (B4) yield

$$\dot{\varepsilon}_p \approx \dot{\varepsilon}_e, \tag{B9}$$

and (28) may be further approximated by

$$\rho_0\theta\dot{\xi}' \approx I_3'^{1/2}\sigma_e\dot{\varepsilon}_e. \tag{B10}$$

APPENDIX C

For simple tension in the $\mathbf{e}_1$ direction of a Cartesian coordinate system the components x_i, F_{iA}, C_{AB} are given by

$$x_1 = aX_1, \qquad x_2 = bX_2, \qquad x_3 = bX_3, \tag{C1a, b, c}$$

$$F_{11} = a, \qquad F_{22} = F_{33} = b, \qquad \text{all other } F_{iA} = 0, \tag{C1d, e, f}$$

$$C_{11} = a^2, \qquad C_{22} = C_{33} = b^2, \qquad \text{all other } C_{AB} = 0. \tag{C1g,h,i}$$

where $a(t)$ is specified and b is determined by the condition that the lateral stresses vanish

$$T_{22} = T_{33} = 0. \tag{C2}$$

It follows from (C1) and the flow rule (11) that the Cartesian components C_{pAB} of $\mathbf{C}_p$ are given by

$$C_{p11} = a_p^2, \qquad C_{p22} = C_{p33} = 1/a_p, \qquad \text{all other } C_{pAB} = 0, \tag{C3a,b,c}$$

where a_p is determined by integrating the only independent equation of (11a) subject to the initial condition (17a). Furthermore, the Cartesian components $(\mathbf{B}_e^{-1})_{ij}$ become

$$(\mathbf{B}_e^{-1})_{11} = (a_p/a)^2, \qquad (\mathbf{B}_e^{-1})_{22} = (\mathbf{B}_e^{-1})_{33} = a_p\, b^2, \qquad \text{all other } (\mathbf{B}_e^{-1})_{ij} = 0. \tag{C4a,b,c}$$

APPENDIX D

In this appendix we approximate the solution of the conditions (36) and the flow rule (11) and show that for pure shear the axial elongation $b-1$ remains small when the material constant $C_2 = -2$. To this end we follow the work of Rubin (1988) on elastic response, neglect terms of order higher than γ_e^2 and approximate the quantities a, b, c, a_p, b_p by

$$a = 1+\tilde{a}\gamma_e^2, \qquad b = 1+\tilde{b}\gamma_e^2, \qquad c = 1+\tilde{c}\gamma_e^2, \qquad a_p = 1+\tilde{a}_p\gamma_e^2, \qquad b_p = 1+\tilde{b}_p\gamma_e^2. \tag{D1a,b,c,d,e}$$

Then, after considerable but straightforward algebra the conditions (36) become

$$\tilde{a}+\tilde{b}+\tilde{c} = -\tfrac{1}{2}C_1\frac{\mu_0}{K_0}(1-m_pK_0), \tag{D2a}$$

$$\tilde{a}-\tilde{a}_p = \left(\frac{2C_2-1}{6}\right)+\tfrac{1}{2}(\tilde{a}+\tilde{b}+\tilde{c}), \qquad \tilde{b}-\tilde{b}_p = \left(\frac{C_2+1}{3}\right)+\tfrac{1}{2}(\tilde{a}+\tilde{b}+\tilde{c}), \tag{D2b,c}$$

and the three independent equations associated with the flow rule (11) become

$$\frac{\mathrm{d}}{\mathrm{d}t}(\tilde{a}_p\gamma_e^2) = \Gamma\left(\frac{C_2-1}{3}\right)\gamma_e^2, \qquad \frac{\mathrm{d}}{\mathrm{d}t}(\tilde{b}_p\gamma_e^2) = \Gamma\left(\frac{C_2+2}{3}\right)\gamma_e^2, \qquad (1+2\tilde{a}_p\gamma_e^2)\dot{\gamma}_p = \Gamma\gamma_e. \tag{D3a,b,c}$$

Multiplying (D2c) by γ_e^2, using (D1b) and integrating (D3b), subject to the initial conditions $\gamma_e = 0$ and $b-1 = 0$, we deduce that

$$(b-1) = \left[\left(\frac{C_2+1}{3}\right)+\tfrac{1}{2}(\tilde{a}+\tilde{b}+\tilde{c})\right]\gamma_e^2+\left(\frac{C_2+2}{3}\right)\int_0^t \Gamma\gamma_e^2\,\mathrm{d}t. \tag{D4}$$

Since the hardening tends to saturate (Fig. 2) the value of γ_e approaches a constant and the first term in (D4) remains small for small elastic distortion. Specifically, from (41), Table 1, and Fig. 2(a, b) near saturation $\gamma_e^2 \approx 1.3\times10^{-3}$ for copper and 6.2×10^{-3} for brass. However, the second term in (D4) continues to increase with time unless the coefficient vanishes ($C_2 = -2$), which explains the results shown in Fig. 3.